

RSC Advances



This is an *Accepted Manuscript*, which has been through the Royal Society of Chemistry peer review process and has been accepted for publication.

Accepted Manuscripts are published online shortly after acceptance, before technical editing, formatting and proof reading. Using this free service, authors can make their results available to the community, in citable form, before we publish the edited article. This *Accepted Manuscript* will be replaced by the edited, formatted and paginated article as soon as this is available.

You can find more information about *Accepted Manuscripts* in the [Information for Authors](#).

Please note that technical editing may introduce minor changes to the text and/or graphics, which may alter content. The journal's standard [Terms & Conditions](#) and the [Ethical guidelines](#) still apply. In no event shall the Royal Society of Chemistry be held responsible for any errors or omissions in this *Accepted Manuscript* or any consequences arising from the use of any information it contains.

Cite this: DOI: 10.1039/c0xx00000x

www.rsc.org/xxxxxx

ARTICLE TYPE

Network Evolutions in both Pure and Silica-Filled Natural Rubber during Cyclic Shear Loading

Fazhong Zhang,^{a,d} Yulong Chen,^{a,d} ChongZhi Sun,^{a,d} Shipeng Wen^{b,d} and Li Liu^{*a,c,d}*Received (in XXX, XXX) Xth XXXXXXXXX 20XX, Accepted Xth XXXXXXXXX 20XX*

DOI: 10.1039/b000000x

Evolutions of chemical cross-linking and filler networks during sinusoidal small-strain (10%) shear loading (fatigue) processes were studied in pure (unfilled) and silica-filled natural rubbers. The experimental results of dynamic mechanical analysis (DMA) and nuclear magnetic resonance (NMR) of pure natural rubber (PNR) indicated that the fatigued PNR has a more homogeneous cross-linking network than that of the virgin one, which can lead to a slightly increase of the storage modulus; however, the change of cross-linking density and its effect on the viscoelastic properties of PNR are very limited. By analyzing the variation of storage and loss moduli and the transmission electron microscopy (TEM) images of silica-filled natural rubber (SFNR) during the cyclic loading process, we found that the loosely packed agglomerates were first disrupted, and then the closed ones could also be gradually broken down. Such a filler network evolution process also can be seen from our non-equilibrium molecular dynamics (NEMD) simulation results.

1. Introduction

Rubber composites (RCs), which are reinforced by fillers, such as carbon black,¹ silica,² and graphene³ and cured by using the technique of accelerated sulfur vulcanization,⁴ are extensively used in industrial applications because of their large elastic deformation and great damping capabilities. Most of the rubber products, such as tires, seals, and engine mounts, are often subjected to cyclic loading conditions in service. Under such conditions, fatigue would happen, which is generally related to the changes of RC structures. In most previous studies, special emphasis was placed on the two distinct processes involved in the fatigue process of RCs: crack nucleation in regions that were initially free of observable cracks and growth of nucleated cracks to the point of failure.⁵⁻⁸ However, there have been few reports about the evolution of material microstructures during cyclic loading.

Rubbers are complicated multi-component systems with both chemical cross-linking and filler network structures.⁹ The cross-linking network formed during the vulcanization of conventional sulfur systems is composed of three types of cross-links: poly-, di-, and mono-sulfidic bonds.¹⁰ Upon application of a stress, the poly-sulfidic bonds are broken before the di- and mono-sulfidic or direct carbon-carbon bonds into short cross-links, such as the di- and/or mono-sulfidic bonds.¹¹⁻¹⁴ The filler network is formed through either direct contact of particles or an adsorbed layer of rubber chains between the fillers.¹⁵⁻¹⁹ Under certain tensile or shearing conditions, the breakdown of the filler network leads to specific nonlinear behaviors of elastomeric materials, such as

strain amplitude dependence of the dynamic viscoelastic properties (Payne effect),^{20,21} hysteresis^{22,23} under cyclic loading, and stress-softening (Mullins effect)^{24,25} at the beginning of cyclic loading. Therefore, investigating the evolutions of both chemical and filler networks during cyclic loading is of prime importance for the comprehension of rubber fatigue mechanisms.

In this study, we first used a combination of various experimental techniques and the non-equilibrium molecular dynamics simulation (NEMD) method to explore the evolutions of chemical and filler networks during long-time cyclic loading conditions. Herein, natural rubber was chosen as matrix, which has outstanding mechanical properties. Silica was chosen as reinforcing filler, which is independent on oil resources and can replace carbon black as an environmentally friendly filler.² Because of the poor compatibility between silica and the rubber matrix, the silane coupling agent was introduced to modify the silica.²⁶ For a running tire, the temperature always reaches up to 60–100 °C because of the hysteresis loss from viscoelasticity of rubber and the frictions among filler–rubber and filler–filler. Therefore, we chose to study the dynamic properties of rubber during fatigue process at temperature of $T = 80^\circ\text{C}$ which can truly reflect many properties of tire in use, such as the rolling resistance. In order to remove the effects of crack initiation and propagation, which are limited for cured rubber subjected to deformations not exceeding about 25%,²⁷ we selected small strain-amplitude (10%) sinusoidal shear deformation as fatigue loading. We start to study the trends of storage modulus (G'), loss modulus (G''), and loss factor ($\tan \delta$) during long-time cyclic loading and the Payne effect at different times of such process of pure (unfilled) natural rubber (PNR) by means of dynamic

mechanical analysis (DMA). Meanwhile, the cross-linking densities at different cycle times were measured by nuclear magnetic resonance (NMR). This way, it was possible to create a clear picture of the evolution of cross-linking network during the cyclic loading process. On this basis, we then investigated the evolution of filler network by analyzing the dynamic viscoelastic properties and the transmission electron microscopy (TEM) images of silica-filled natural rubber (SFNR) during cyclic loading after discriminating the effect of chemical network. Finally, NEMD, from which the microscopic dispersion can be calculated,²⁸⁻³² was employed to verify the evolution of the filler network.

2. Materials and methods

2.1. Materials and sample preparation

Natural rubber (NR), RSS-3, was obtained from Hatyai Rubber Market, Thailand; precipitated silica of Ultrasil VN3 (pH 5.4–7.0, surface area 175 m²/g, average diameter 20 nm) was produced by Evonik Degussa (China) Co., Ltd; and other materials such as vulcanization activators (zinc oxide and stearic acid), antioxidants (N-isopropyl-N'-phenyl-1,4-phenylenediamine (4010NA)), silane coupling agent (bis[3-(triethoxysilyl)propyl]tetrasulfide (TESPT)), vulcanizing agent (sulfur (S)) and accelerators (2,2'-benzothiazyl disulfide (DM) and 4,4'-dithiodimorpholine (DTDM)) were purchased from the market.

Both the PNR and SFNR samples were obtained by a standard mixing/curing procedure. During the mixing procedure, NR 100 phr (phr means per hundred rubber), zinc oxide 5 phr, stearic acid 1 phr, and 4010NA 2 phr were first blended using a two-roll mill with a friction ratio of 1:1.35. For the SFNR samples, 50 phr of precipitated silica and 4 phr of TESPT were also incorporated into the above blend and mixed until almost well dispersed. Then, S 1.2 phr, DM 1.0 phr, and DTDM 3.0 phr were added and further blended for 3–4 min. Room temperature (below 30 °C) was maintained during the milling process to avoid early cross-linking reaction. The milled rubber stayed for 24 h prior to curing. The uncured rubber sheets were vulcanized under press at 143 °C in 2 mm thick plates for an optimum time (about 15 min), which was determined by a disc rheometer (Model 750, Beijing Huanfeng Chemical Machinery Experimental Factory).

2.2. Experiments

2.2.1. Dynamic Mechanical Analysis Measurements.

All the dynamic measurements were performed on a VA 3000 DMA (01-dB Metravib Company, France). Test strips were cut from the cured rubber sheets, about 1.5 cm wide and 3 cm long. A sinusoidal shear strain with amplitude of 10% and frequency of 10 Hz was applied on both the PNR and the SFNR strips for different cyclic loading cycles by using the shear fatigue mode of the DMA. The test temperature was fixed at 80 °C. The steady-state stress responses were evaluated in terms of G' , G'' and $\tan \delta$. The

specimens with different degrees of fatigue were then used for shear strain sweeping test on the same equipment under the same frequency and temperature to probe their network structures. For comparison, a virgin specimen (without any fatigue treatment) was also used for the strain sweeping test. Similarly, the stress responses to the strain excitations were recorded automatically, and from these measurements the amplitude dependence of the G' , G'' and $\tan \delta$ were calculated.

2.2.2. Cross-linking Density Measurements.

Cross-linking density (XLD) measurements were carried out by using NMR relaxation technique, a convenient method for characterizing polymer networks, on a IIC XLDS-15 cross-linking density spectrometer (IIC Innovative Imaging Corp. KG, Germany). Samples were cut from both the virgin and fatigue treated PNR strips and placed into glass tubes. The samples were approximately 8 mm in length and 5 mm in diameter. The measurement temperature was 60 ± 0.1 °C. The XLD measurements were based upon the analysis of the shape and time constant of the magnetization decay of the hydrocarbon protons obtained by spin-echo measurements. The signal decay in chemical cross-linking network obeys the Gaussian-exponential function expressed as $M(t) = A_0 + A_1 \exp[-t/T_2 - 1/2(qM_2T_2)] + A_2 \exp(-t/T_2)$, where $M(t)$, the detected signal, corresponds to the magnetization decay function, A_0 compensates for a possible offset of the signal, A_1 represents the amplitude of the rigid fraction of network, A_2 represents the relative amount of the mobile fraction of polymer, T_2 corresponds to the spin-spin relaxation time, qM_2 is the remaining dipolar magnetic coupling of the hydrocarbon chain protons as a consequence of the anisotropic motion of the chain segments and it is the parameter that allows determination of the average molecular weight between chemical cross-linking bonds, M_c .^{33,34} Because of the increased XLD upon crosslink, the degree of molecular motion decreases, with a consequent slight decrease of the spin-spin relaxation time T_2 ; therefore, the higher the XLD, the lower the T_2 . The time signal has been used for data analysis. Each signal decays covered 512 data points at an acquisition time of 10.24 msec. For determination of the relaxation time T_2 , 64 measurements at different times were carried out. Data analysis was performed with the IIC Analysis Software package, using a nonlinear Marquardt-Levenberg algorithm.

2.2.3. Transmission electron microscopy (TEM).

Ultra-thin sections of composite samples (the SFNR strips treated by DMA at different fatigue time) for TEM observations were cut by a liquid-nitrogen-cooled microtome at -100 °C, collected on a copper grid, and then observed on a JEOL JEM-3010 high-resolution transmission electron microscope at an acceleration voltage of 200 kV.

2.3. Simulations

To provide an intuitive insight into the evolution of filler network during the fatigue process, NEMD was employed in this work by using the large scale atomic/molecular massively parallel

simulator (LAMMPS)³⁵ molecular dynamics package. The simulated system contained 150 Kremer-Grest³⁶ bead-spring polymer chains with degree of polymerization $N = 80$. All of the monomers interacted through the Lenard-Jones (LJ) potential truncated and shifted at $r_c = 2 \times 2^{1/6} \sigma$ (where σ is the distance unit in our simulation). Adjacent chain monomers were bonded by a finitely extendible nonlinear elastic (FENE) model potential. The system composed of 48 initially clustered filler particles that were modelled as spheres with diameter of 4σ . The polymer–filler and filler–filler interactions are similar with the simulation of Smith et al.,³⁷ but with energy parameters between polymer and filler particle (ϵ_{np}) equal to 10.0ϵ and between filler particles (ϵ_{mn}) equal to 2.0ϵ , and their cutoffs being 2.5σ . The simulation cell is a cubic box with a length of $\sim 25\sigma$. The polymer monomer density was about 0.85, and the filler volume fraction ϕ was about 10.2%. Periodic boundary conditions were used in all three spatial directions. In addition, chemical bonds between adjacent polymer chains were formed to crosslink the polymer matrix, and the cross-linking density was $\rho_{cl} = N_{cl}/V = 0.075\sigma^{-3}$, where N_{cl} is the number of cross-linking bonds and V is the volume of the simulation box. It has been reported that when mapping the coarse-grained bead–spring model to real polymer, the length σ is about 0.5 to 1.3 nm.³⁶ Correspondingly, the cross-linking density of our simulation systems is about 5.5×10^{-5} to 9.6×10^{-4} mol/cm³, highly in accordance with real situation (also in the range of 10^{-5} to 10^{-4} mol/cm³). A cyclic shear deformation with strain amplitude of 10% was then applied to the system for sufficient time by using the SLLOD algorithm^{38,39} in conjunction with a continuously deforming, non-orthogonal simulation box.⁴⁰ The configurations in each cyclic period were collected when the simulation box returned to its originally cubic shape. Detailed simulation models and method can be found in our recent work.⁴¹

3. Results and discussion

3.1. Evolution of chemical network

The dynamic properties of PNR during fatigue, as shown in Figure 1, were recorded by DMA. The G' decreases by 0.1 kPa in the first 1 000 cycles (curve a), indicating that the material exhibits a slight softening behaviour at the beginning of the cyclic loading. However, after this short stage, the G' increases with further increases in the number of cycles. The initial decrease in material stiffness, which is also referred to as the Mullins effect, is believed to be associated with the removal of entanglements and the breakage of weak bonds, such as poly-sulfidic bonds, in unfilled rubber.²⁵ After the majority of the poly-sulfidic bonds have been broken up and gradually converted into di- and/or mono-sulfidic bonds, the G' increases. Additionally, the orientation of chain segments and the cross-linking network becomes more and more uniform during the above process, which make the material can hold more stress, also contribute to the increase of G' . Note that the variation range of G' during the fatigue process are within the value of 0.9 kPa, indicating that the change of cross-linking density is limited to a low level. Meanwhile, the G'' (curve b) and the $\tan \delta$ (curve c) are low and show no obvious changes at all number of cycles because the

energy dissipation caused by chain sliding or entanglement-disentanglement effect is limited and hardly changes during the fatigue process.

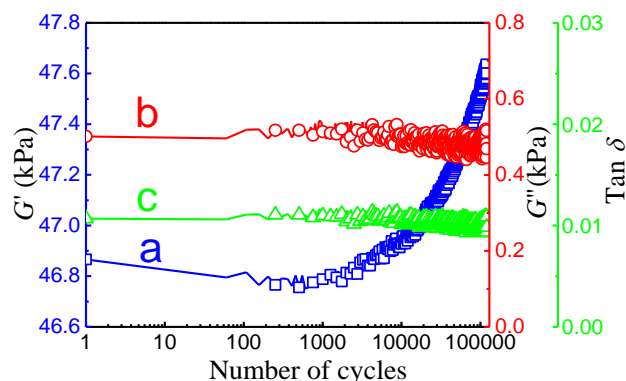


Figure 1. (a) Storage modulus (G'), (b) loss modulus (G''), and (c) loss factor ($\tan \delta$) of PNR as a function of cyclic number. The test conditions of the shear fatigue test are as follows: the test temperature is 80°C, strain amplitude is 10%, cyclic frequency is 10Hz, and cyclic number is 120 000.

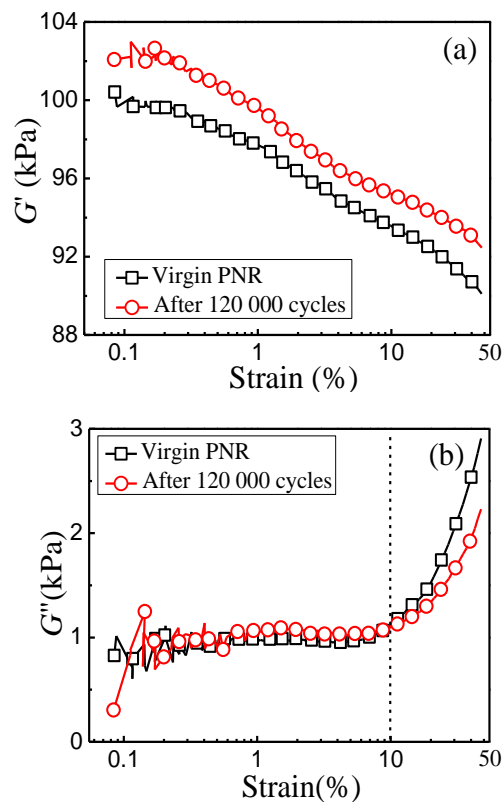


Figure 2. Strain-amplitude dependence of (a) storage modulus (G') and (b) loss modulus (G'') of virgin PNR and PNRs pre-treated for 120 000 fatigue loading cycles.

The variations in the G' and the G'' with strain amplitude of the virgin PNR and PNR pre-treated for 120 000 cycles of fatigue loading are presented in Figure 2. As shown in Figure 2a, the G' is a little higher for the pre-treated PNR than for the virgin PNR, further demonstrating that the fatigued PNR has a more homogeneous cross-linking network and more oriented

arrangement of molecular chains, and thus can support a higher external loading. In Figure 2b, both the virgin and the fatigued PNR have similar plateaus in the plot of G'' versus strain at strain amplitudes lower than 10%. However, at strain amplitudes higher than 10%, the G'' increases sharply, and the G'' of the fatigued specimen is lower than that of the virgin specimen, suggesting that for the virgin sample the physical interactions between the rubber chains can be further disrupted at strain amplitudes higher than 10%. For example, the entanglement and disentanglement of rubber chains can be greatly enhanced under high strain amplitude cyclic loading. But for the fatigued PNR, the more homogeneous cross-linking network leads to lower breaking and reforming rates of the weak physical interactions between the polymer chains and results in a lower G'' than that of the virgin PNR at the same strain amplitude.

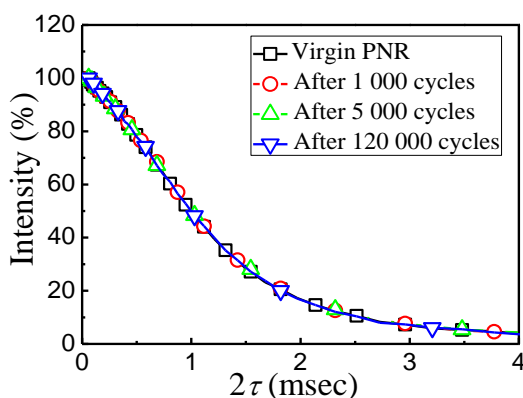


Figure 3. Signal decay in the chemical cross-linking network, obtained by NMR, of PNR for various degrees of fatigue.

To quantitatively characterize the cross-linking density of PNR as a function of fatigue cycles, we studied the signal decay in the chemical cross-linking network of PNR for various degrees of fatigue by means of NMR, and the results are shown in Figure 3. All the curves almost overlap on each other, indicating that the total number of chemical cross-linking bonds shows no noticeable difference before and after fatigue. This observation suggests that the weak chemical bonds, such as poly-sulfidic bonds, can be broken up under cyclic loading and gradually converted into di- and/or mono-sulfidic bonds, and thus making the total number of cross-linking bonds nearly unchanged. As a result, a more homogeneous chemical network is formed, increasing the storage modulus of the fatigued PNR.

3.2. Evolution of filler network

Under the same DMA fatigue test conditions as those for the PNR, we studied the dynamic behaviour of SFNR during 120 000 cycles of cyclic loading and the results are shown in Figure 4. Similar to the results of PNR (Figure 1), the G' of SFNR first decreases in Stage 1 and then significantly increases in Stage 2 (curve a). During such a process, the TEM images of the sample at different fatigue time also be characterized and presented in Figure 5. The breakage of large silica agglomerates (see TEM images a and b, in Figure 5) and the release of confined rubber chains on the filler surfaces are probably responsible for the

decrease of G' in Stage 1. As the filler agglomerates are broken into small ones or even single silica particles during the fatigue process, the rubber chains tend to penetrate into the agglomerates by overcoming the physical interactions between the fillers with the aid of cyclic shear force. Consequently, with increasing degree of fatigue, the silica particles are dispersed much more uniformly (see TEM image c, in Figure 5), and the rubber chains linking the silica particles appear to be more perfectly oriented, resulting in the increase of G' . The above conclusions also can be intuitively depicted by the schematic view displayed in Figure 5. This phenomenon is different from the results of Mars and Fatemi⁴² in which they explored multiaxial stress effects on fatigue crack nucleation and growth in carbon black-filled NR based on experiments using short thin-walled cylindrical specimens subjected to axial and twist displacements and found that when strain amplitude larger than 40%, the crack growth happens at the last stage of the test, leading to the decrease of G' . However, the crack growth would not occur in our present study during the 120 000 cycles of fatigue loading with such low strain amplitudes (10%). It should be noted that the range of G' , i.e., $G'_{\max} - G'_{\min}$, of SFNR is almost 30 times larger than that of PNR. The much larger variation of G' of SFNR than that of PNR shows that G' strongly depends on the filler network in SFNR.

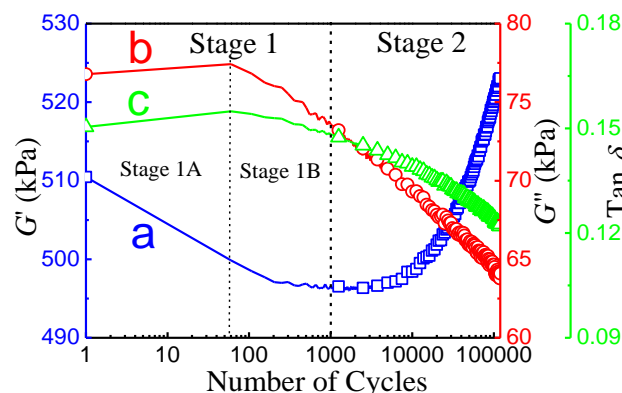


Figure 4. (a) Storage modulus (G'), (b) loss modulus (G''), and (c) loss factor ($\tan \delta$) of SFNR as a function of number of cycles. The test conditions for the shear fatigue test are as follows: the set temperature is 80 °C, strain amplitude is $\pm 10\%$, cyclic frequency is 10 Hz, and number of cycle is 120 000.

The G'' of SFNR also shows some evident changes. In Stage 1A, i.e., the first 60 cycles, the G'' slightly increases, but after this short initial stage, G'' (curve b) and $\tan \delta$ (curve c) both decrease continuously. The initial slight increase of G'' is related to the enhancement of the cyclic breaking and reforming of physical filler–filler bonds in filler agglomerates.⁴³ With fatigue proceeding, some of the agglomerates, especially the loosely packed ones, gradually be broken into small agglomerates or isolated particles and unable to be agglomerated again when the rubber chains have penetrated into the gaps among these filler particles, resulting in the improvement of filler dispersion. This will weaken the breaking and reforming of physical filler–filler bonds, leading to the decrease of G'' and $\tan \delta$.

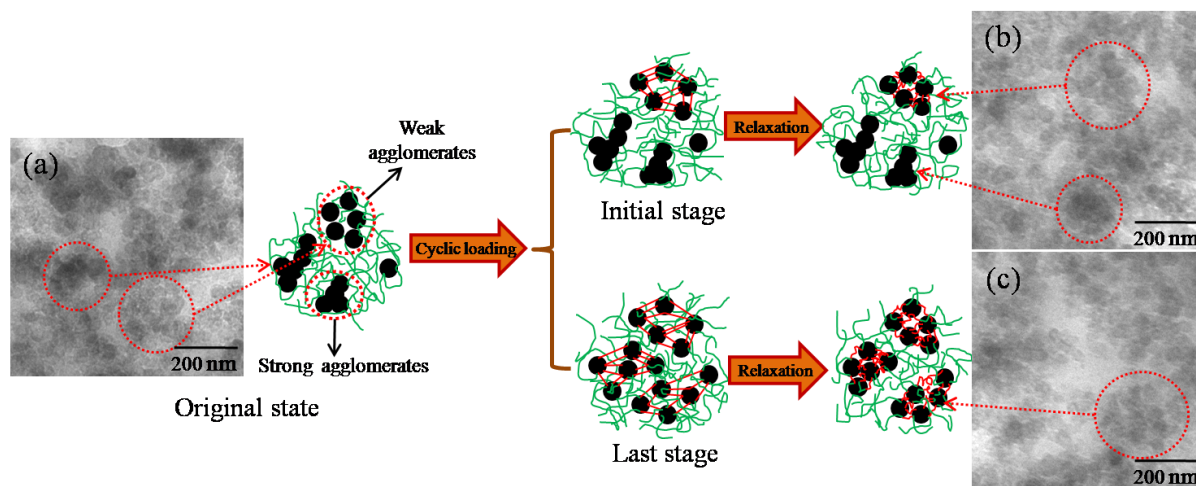


Figure 5. TEM images and schematic view for the evolution of filler network in SFNRs at different fatigue time: (a) original state, (b) initial stage (1000 cycles), and (c) last stage (100 000 cycles).

The specimens after cyclic shearing test of varied fatigue loading cycles were then used to carry out the strain sweeping test. Additionally, the virgin SFNR was also included for comparison. It is important to note that the transition time between different test modes is short, but it is long enough for the molecular configurations in SFNR to relax. As shown in Figure 6a, the G' of all samples gradually decreases within the whole range of strain amplitudes (ranging from 0.1% to 50%). This phenomenon is often referred to as the Payne effect in filled rubbers. We also found that the G' of the sample after 1000 fatigue cycles is lower than that of the virgin sample at all strain amplitudes, because the large filler agglomerates are broken down to release the trapped rubber in the filler agglomerates. Thus, the effective filler volume fraction and hence the modulus decrease.⁴⁴ While when the fatigue loading cycles ranging from 1000 to 3000, the curves almost overlap on each other, as shown in the insert of Figure 6. However, with the cyclic number increasing beyond 4 000, many more filler agglomerates are broken down, and more rubber chains are stretched between filler particles. These stretched chains would recover to random-coil configurations during the transition between test modes because of the effect of entropy increase, and thus the filler particles linked by these chains tend to re-agglomerate (see Figure 5). These re-agglomerative filler structures are looser than that of the virgin SFNR, in which more rubber chains exist among the filler particles and bonded these particle together. These structures will increase the G' of the specimen in the strain sweep test because of the chain orientation effect between the filler particles. Therefore, when the number of cycles exceeds 3000, the higher the degrees of fatigue of the specimens, the higher the G' ; in particular, the G' of the sample after 120 000 fatigue cycles is even higher than that of the virgin sample.

The strain amplitude dependence of the loss modulus G'' is displayed in Figure 6b. The G'' of most of the samples, except the one after 120 000 fatigue cycles, first increase and then decrease with increasing strain amplitude. The mechanism of this phenomenon is as follows: With the increase of strain amplitude, more and more filler agglomerates are broken down by shear force, while the attractive interactions as well as the rubber chains

linked between the fillers contribute to filler agglomeration, and the de-agglomeration and agglomeration process will increase G'' . However, as the strain amplitude exceeds a certain value, the broken filler agglomerates are unable to re-agglomerate, resulting in the decrease of G'' .

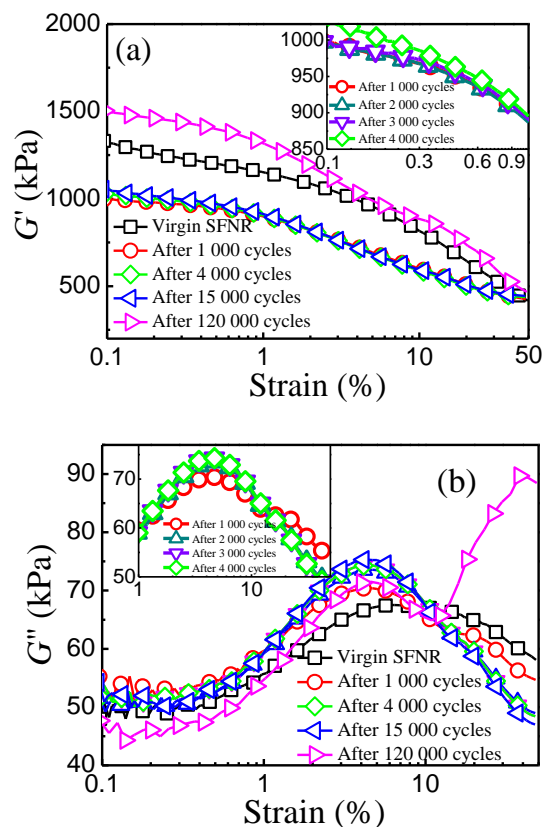


Figure 6. Strain-amplitude dependence of (a) storage modulus (G') and (b) loss modulus (G'') of virgin SFNR and SFNRs pre-treated for different numbers of fatigue cycles (1000, 4000, 15 000, and 120 000 cycles).

In addition, with the increase in the degree of fatigue of the specimen (except for the specimen with 120 000 fatigue cycles), the peak of the plot of G'' versus strain amplitude becomes higher,

while its width becomes narrower. The agglomeration of filler particles on a large scale results in the formation of filler clusters with various sizes, including the infinite filler network.⁴⁵ Some clusters are closely packed to form agglomerates with strong particle–particle interactions, while some have loose packing structures, and some are even mono-dispersed in the rubber matrix. Upon the application of constant-amplitude cyclic shear deformation, the weak agglomerates tend to be broken prior to the strong ones. During the breaking of the agglomerates, the rubber chains in the vicinity of them penetrate into their gaps and are adsorbed on the silica surfaces. With more and more chains penetrating into these gaps, the filler particles are gradually dispersed into the matrix. When the number of cycles further increases, the strong agglomerates can also be loosened. The rubber chains linking the dispersed filler particles will be stretched and oriented. This oriented state is a quite unstable and transient, with lower entropy than that of the quiescent systems. If the external loading is removed, under the driving force of entropy increase, the rubber chains linked to filler particles shrink into random-coil states, and the linked filler particles will quickly agglomerate again. These re-agglomerated filler agglomerates have looser structures than the never broken ones. Therefore, the SFNR samples with different degree of fatigue should have different filler network structures. The distribution of distances between filler particles in SFNR is narrowed after fatigue (though the distribution pattern has not been determined up to date), apparently resulting in a higher and narrower G'' peak with increasing number of cycles.

For the specimen after 120 000 fatigue cycles, a similar phenomenon to that of specimens subjected to lower degrees of fatigue appears at strains below 10%. However, the G'' of this specimen, even though higher than that of a virgin specimen, become lower than that of other specimens with low degree of fatigue. Moreover, the G'' increases significantly with increasing strains over 10%. The specimen after a long fatigue process probably has a structure in which the fillers are well dispersed (even mono-dispersed) in the rubber matrix with rubber chains linking them. Such a structure has low energy dissipation at small strains because the fillers are less likely to de-agglomerate and re-agglomerate. As the strain exceeds a critical value, the rubber chains linking the fillers will be stretched, making these chains more ordered. The order-disorder transformation of chain structure during the cyclic process would consume a large amount of energy, leading to the increase of G'' .¹⁰

Furthermore, NEMD was used to verify the above observations. The intuitive snapshots and the average number of neighboring nanoparticles (NPs) within a distance of $L = 5.5\sigma$ from a given NP are shown in Figure 7a and b, respectively. Note that a good dispersion will lead to a low value of the number of neighboring NPs.⁴⁶ In our simulation, all of the NPs are initially clustered as a large agglomerate as shown in Figure 7a. As the cyclic shear deformation is imposed, the filler agglomerates are gradually broken down during the initial 1000 cycles (Figure 7a). Correspondingly, the number of neighboring NPs decreases with increasing number of cycles, as shown in Figure 7b. During this process, the matrix polymer chains also gradually penetrate into the aggregations and are adsorbed on the NP surfaces, thus separating the NPs. As the dynamic fatigue process goes on, the

NPs are continuously dispersed into the polymer matrix until the filler network reaches a steady state with a well-dispersed filler structure. As shown in Figure 7a and b, the snapshots and the number of neighboring NPs hardly change after 1000 simulation cycles.

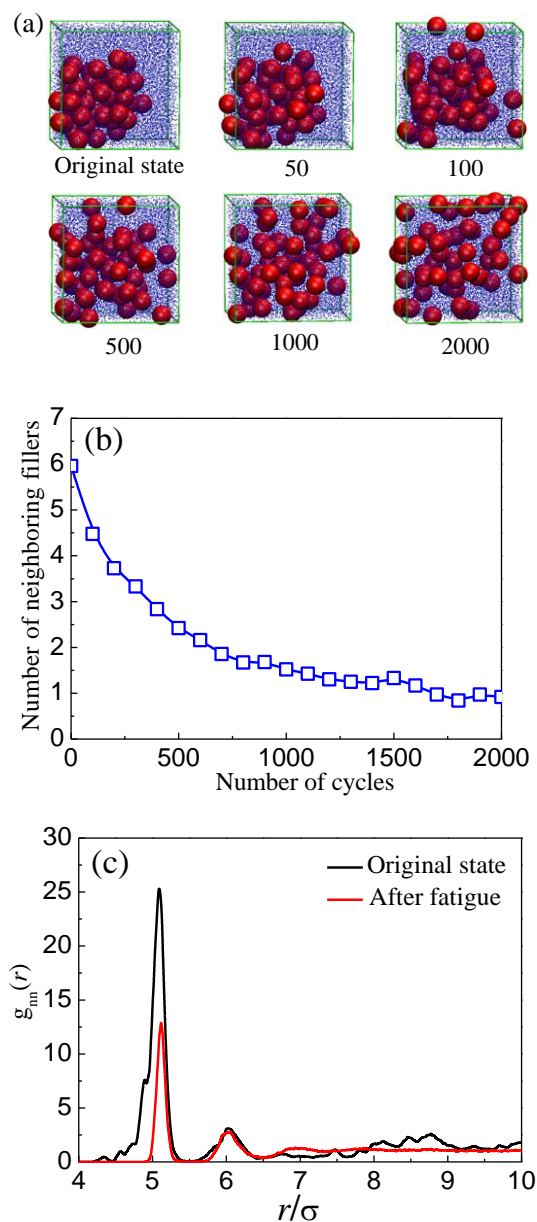


Figure 7. (a) Snapshots of dynamic evolution process of filler network during cyclic shear deformation for different fatigue cycles. The red spheres represent the filler particles, and the blue dots represent the polymer chains. (b) Average number of neighboring filler particles within a distance of 5.5σ from filler particles as a function of number of cycles. (c) Comparison of the NP–NP radial distribution functions, $g_{nn}(r)$, for the systems of the initial state and the final state after fatigue.

We also compared the NP spatial distribution of the systems before and after fatigue by characterizing their radial distribution functions (RDF) between the NPs, where $g_{nn}(r)$ represents the number density of the NPs, which are apart from a given NP at distance r normalized by mean number density, as shown in Figure 7c. We can find that there are mainly two peaks appear at

$r = 5\sigma$ and 6σ , respectively, for both the initial system and the final system after fatigue. Note that the peak at $r = 5\sigma$ for the initial system is much wider and higher than that for the final system. In addition, this peak also starts from a lower distance r . These observations indicate that the NPs in the initial system are more closely packed. During the fatigue process, the NPs structure can be gradually broken down, leading to the decrease of the peak. Moreover, the polymer chains also can continuously penetrate into the gaps between the filler particles during the fatigue process, resulting in a large separation between the NPs as the peak gradually shifted to the right at x -axis. These observations are in excellent agreement with our experimental result.

4. Conclusions

We have studied the evolutions of both chemical cross-linking and filler networks during the cyclic shear loading fatigue processes by using various experimental techniques and the NEMD method. We observed that the cross-linking density of PNR during the long-time fatigue process hardly changes. The evolution of cross-linking network, that is, the poly-sulfidic bonds, would be broken up and gradually converted into di- and/or mono-sulfidic bonds, resulting in the formation of a uniform chemical network, with minimal change in the viscoelastic properties of PNR. This observation is a prerequisite to study the evolution of filler network in reinforced materials because we can discriminate and quantify the effect of chemical network on viscoelastic properties of SFNR. Our results showed that during the fatigue process, the loosen silica agglomerates are first disrupted and the closed ones could also be gradually broken down, and the filler particles would become more and more homogeneous. The reformed agglomerates are looser than those have never been broken. Therefore, the structures of the rebuilt filler networks are highly dependent on the degree of fatigue. For the materials with the agglomerates broken down by cyclic shear forces, the filler particles would form some new agglomerates with similar sizes and almost the same distance between adjacent particles. The materials with such structures should exhibit unique strain-amplitude-dependent viscoelastic properties different from those of the original materials. Meanwhile, our molecular simulation results also support the above conclusions, even though some simplifying assumptions were made in the simulations, for instance, the NPs are with the same size and sphere shape, the polymer chains still cannot map the specific rubbers, and so on. Therefore, simulations with more realistic models than those used in this study and experimental techniques with the ability of detecting the microstructures of materials during high frequency cyclic loading processes need to be developed. Nevertheless, the results in current study can provide some significant understanding of fatigue mechanism on a microscopic scale.

Acknowledgements

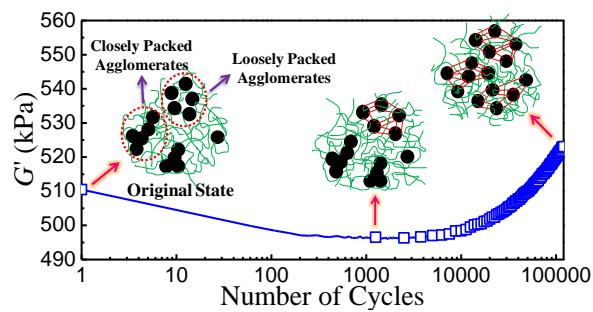
This work was supported by CHEM-CLOUD-COMPUTING and the Natural Science Foundation of China (No: 51073008 and 51103005).

Notes and references

- ^a State Key Laboratory of Chemical Resource Engineering, Beijing University of Chemical Technology, Beijing 100029, China.
- ^b State Key Laboratory of Organic-Inorganic Composites, Beijing University of Chemical Technology, Beijing 100029, China.
- ^c Key Laboratory of Carbon Fiber and Functional Polymers, Ministry of Education, Beijing University of Chemical Technology, Beijing 100029, China.
- ^d Beijing Engineering Research Center of Advanced Elastomers, Beijing University of Chemical Technology, Beijing 100029, China.
- * Corresponding author. E-mail: LiuL@mail.buct.edu.cn; Fax: +86-10-64433964; Tel: +86-10-64443413.
- 1 G. Kraus, In *Fortschritte der Hochpolymeren-Forschung*, 1971, vol. 8, pp. 155.
- 2 A. Voet, J. C. Morawski and J. B. Donnet, *Rubber Chem. Technol.*, 1977, **50**, 342–355.
- 3 Y. Mao, S. Wen, Y. Chen, F. Zhang, P. Panine, T. W. Chan, L. Zhang, Y. Liang and L. Liu, *Sci. Rep.*, 2013, **3**, 2508.
- 4 M. R. Krejsa and J. L. Koenig, *Rubber Chem. Technol.*, 1993, **66**, 376–410.
- 5 W. V. Mars and A. Fatemi, *Int. J. Fatigue*, 2002, **24**, 949–961.
- 6 J. B. Le Cam, B. Huneau, E. Verron and L. Gornet, *Macromolecules*, 2004, **37**, 5011–5017.
- 7 H. Zhang, A. K. Scholz, J. de Crevoisier, F.–L. Vion, G. Besnard, A. Hexemer, H. R. Brown, E. J. Kramer and C. Creton, *Macromolecules*, 2012, **45**, 1529–1543.
- 8 J. B. Le Cam and E. Toussaint, *Macromolecules*, 2010, **43**, 4708–4714.
- 9 W. F. Reichert, D. Göritz and E. J. Duschl, *Polymer*, 1993, **34**, 1216–1221.
- 10 J. Shen, S. Wen, Y. Du, N. Li, L. Zhang, L. Yang and L. Liu, *Radiat. Phys. Chem.*, 2013, **92**, 99–104.
- 11 G. J. Lake and P. B. Lindley, *J. Appl. Polym. Sci.*, 1965, **9**, 1233–1251.
- 12 H. Chun and A. N. Gent, *Rubber Chem. Technol.*, 1996, **69**, 577–590.
- 13 W. V. Mars and A. Fatemi, *Rubber Chem. Technol.*, 2004, **77**, 391–412.
- 14 M. D. Ellul, In *Engineering with Rubber – How to Design Rubber Components*, ed. A. N. Gent, 3rd edn., 2012, pp. 137.
- 15 N. Jouault, P. Vallat, F. Dalmás, S. R. Said, J. Jestin and F. O. Boué, *Macromolecules*, 2009, **42**, 2031–2040.
- 16 G. Capuano, G. Filippone, G. Romeo and D. Acierno, *Langmuir*, 2012, **28**, 5458–5463.
- 17 N. Jouault, F. Dalmás, F. Boué and J. Jestin, *Polymer*, 2012, **53**, 761–775.
- 18 M. I. Aranguren, E. Mora, V. Jon, J. DeGroot and C. W. Macosko, *J. Rheol.*, 1992, **36**, 1165–1182.
- 19 S.–S. Choi, B.–H. Park and H. Song, *Polym. Adv. Technol.*, 2004, **15**, 122–127.
- 20 A. R. Payne, *J. Appl. Polym. Sci.*, 1962, **6**, 57–63.
- 21 A. R. Payne and R. E. Whittaker, *Rubber Chem. Technol.*, 1971, **44**, 440–478.
- 22 D. F. Moore and W. Geyer, *Wear*, 1974, **30**, 1–34.
- 23 J. S. Bergström and M. C. Boyce, *Mech. Mater.*, 2000, **32**, 627–644.
- 24 L. Mullins, *Rubber Chem. Technol.* 1969, **42**, 339–362.
- 25 J. Diani, B. Fayolle and P. Gilormini, *Eur. Polym. J.*, 2009, **45**, 601–612.
- 26 Y. Li, B. Han, L. Liu, F. Zhang, L. Zhang, S. Wen, Y. Lu, H. Yang and J. Shen, *Compos. Sci. Technol.*, 2013, **88**, 69–75.
- 27 A. I. Medalia, *Rubber Chem. Technol.*, 1978, **51**, 437–523.
- 28 F. W. Starr, J. F. Douglas and S. C. Glotzer, *J. Chem. Phys.*, 2003, **119**, 1777–1788.
- 29 V. Kalra, F. Escobedo and Y. L. Joo, *J. Chem. Phys.*, 2010, **132**, 024901.
- 30 J. D. Thomin, P. Keblinski and S. K. Kumar, *Macromolecules*, 2008, **41**, 5988–5991.
- 31 E. Jaber, H. Luo, W. Li and D. Gersappe, *Soft Matter*, 2011, **7**, 3852–3860.
- 32 G. Raos and M. Casalegno, *J. Chem. Phys.*, 2011, **134**, 054902.
- 33 H. Du, Y. Yu, G. Jiang, J. Zhang and J. Bao, *Macromol. Chem. Phys.*, 2011, **212**, 1460–1468.
- 34 G. Simon, K. Baumann and W. Gronski, *Macromolecules*, 1992, **25**, 3624–3628.

- 35 S. Plimpton, *J. Comput. Phys.*, 1995, **117**, 1–19.
- 36 K. Kremer and G. S. Grest, *J. Chem. Phys.*, 1990, **92**, 5057–5086.
- 37 J. S. Smith, D. Bedrov and G. D. Smith, *Compos. Sci. Technol.*, 2003, **63**, 1599–1605.
- 5 38 D. J. Evans and G. P. Morriss, In *Statistical Mechanics of Nonequilibrium Liquids.*, Academic Press: London, 1990; p 328.
- 39 M. E. Tuckerman, C. J. Mundy, S. Balasubramanian and M. L. Klein, *J. Chem. Phys.*, 1997, **106**, 5615–5621.
- 40 C. M. Tenney and E. J. Maginn, *J. Chem. Phys.*, 2010, **132**, 014103.
- 10 41 Y. Chen, L. Liu, Q. Yang, S. Wen, L. Zhang and C. Zhong, *Langmuir*, 2013, **29**, 13932–13942.
- 42 W. V. Mars and A. Fatemi, *Int. J. Fatigue*, 2006, **28**, 521–529.
- 43 G. Heinrich and M. Klüppel, *Adv. Polym. Sci.*, 2002, **160**, 1–44.
- 44 M.-J. Wang, *Rubber Chem. Technol.*, 1999, **72**, 430–448.
- 15 45 G. Heinrich, M. Klüppel and T. A. Vilgis, *Curr. Opin. Solid State Mater. Sci.*, 2002, **6**, 195–203.
- 46 J. Liu, Y. Gao, D. Cao, L. Zhang and Z. Guo, *Langmuir*, 2011, **27**, 7926–7933.

Graphical Abstract



5 **Text:** During fatigue process, the loosen silica agglomerates are first disrupted and then the closed ones also be gradually broken down, and the filler particles would become more and more homogeneous

10